Research Article Vol. 2, No. 2 / 15 Feb 2023 / Optics Continuum 484
OPTICS CONTINUUM

Towards true volumetric refractive index investigation in tomographic phase microscopy at the cellular level

MARIA BACZEWSKA,* MARTYNA MAZUR, AND WOJCIECH KRAUZE

Warsaw University of Technology, Institute of Micromechanics and Photonics, ul. Sw. A. Boboli 8, Warsaw, 02-525, Poland
*maria.baczewska.dokt@pw.edu.pl

Abstract: Tomographic phase microscopy (TPM) is one of the most widely used quantitative phase imaging techniques. It is a non-invasive, label-free technique that allows high-resolution imaging. It enables the morphology of a living cell to be captured without chemical treatment, by using the refractive index (RI) as a contrast parameter to image internal structures. In this paper, we demonstrate that due to the fact that biological cells are highly heterogeneous structures, it is crucial to use full volumetric data to calculate the average RI values of biological samples and their organelles. To prove our point, we present tomographic reconstructions of 3 cell types: neuroblastoma SH-SY5Y, adenocarcinoma A549 and leukemia HL-60, from which we calculate the average RI value from the 3D volumetric data and compare it to the average RI values calculated from each 2D section.

1. Introduction

Tomographic phase microscopy (TPM) is a label-free, high-resolution and non-invasive method for obtaining three-dimensional refractive index (RI) distribution of analyzed biological samples [1,2]. It allows capturing the morphology of a living cell without chemical processing - RI is used as a contrast parameter to image internal structures [3–5]. The knowledge about average RI within a cell volume or the volume of its substructure can be used to calculate its dry mass. One aspect that can be observed is that often only one 2D lateral (XY) cross-section through the 3D tomographic reconstruction is used to image the distribution of RI in a cell and calculate the average RI [2,6], ignoring the volumetric information that TPM provides. This is due to the fact that nowadays most of TPM devices are 'limited angle' systems that provide results with 'missing cone' artifacts and are utilizing high numerical aperture objectives [7,8]. This means that only a thin region surrounding the central XY cross-section that is conjugated with the camera has high quality [9]. There are multiple numerical algorithms that are designed to minimize these artifacts [10–13]. All of them, however, are time-consuming, so it is often preferred to use fast methods that ignore 'limited angle' nature of the measurement [14] or present only the results from 1 cross-section [4]. However, cells are highly heterogeneous objects, so selecting and calculating the average RI based on a single cross-section can result in omitting structures located at other heights and falsifying the RI value of the whole cell. Also, despite high visual quality of the cross-section, its RI values are underestimated, unless specialized algorithms are used [15]. Again, this results in erroneously calculated dry mass.

In our work, we aim to demonstrate the importance of using RI information from the whole cell volume. To prove our point, we present tomographic reconstructions of 3 cell types: SH-SY5Y neuroblastoma, A549 adenocarcinoma and HL-60 leukemia, from which we calculate the average RI value from 3D volumetric data and compare it with average RI values calculated from each 2D cross-section.

#481162 https://doi.org/10.1364/OPTCON.481162
Journal © 2023 Received 16 Nov 2022; revised 10 Jan 2023; accepted 10 Jan 2023; published 15 Feb 2023

OPTICS CONTINUUM

2. Methods

2.1. Tomographic phase microscopy system

The 3D RI distribution of cells was measured using a tomographic phase microscopy (TPM) system based on a Mach-Zehnder interferometer (Fig. 1(A)). 90 projections of the sample were captured with 633nm laser illumination. To provide a set of projections obtained at different angles without moving the measured object, the system used two high numerical aperture microscope objectives (for both MO1 and MO2, NA=1.3) and a galvanometer mirror (GM). Cells were measured directly in the medium with refractive index $n = 1.338$. This allows a maximum illumination angle ranging up to 45°. Theoretical lateral and axial resolution was 0.12 µm and 0.3 µm, respectively [16]. The complete description of the system can be found in [17].

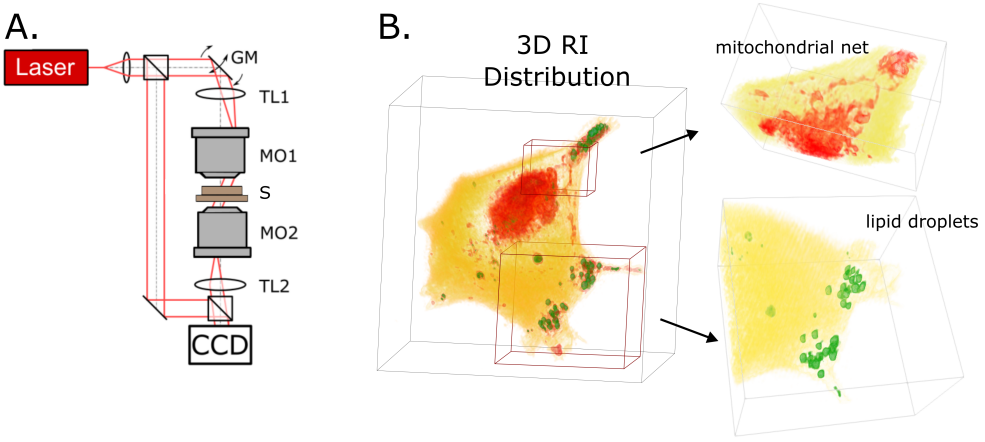

Fig. 1. A. Tomographic phase microscopy system (TL1, TL2 - tube lenses; MO1, MO2 - microscope objectives; S - sample, GM - galvanometer mirror); B.3D tomographic reconstruction with magnified regions showing different structures withing cell volume.

2.2. Tomographic reconstruction methods

Two algorithms were used to reconstruct the RI distribution of analysed samples from the measured projections: (1) single-step Direct Inversion (DI) algorithm for fast reconstruction without any artifact compensation that are due to limited angular range of projections (so called missing cone) and (2) iterative version of DI method, called Gerchberg-Papoulis with finite object support (GPSC) [11]. In GPSC, there are 2 constraints used in every iteration: nonnegativity and object support, which is an advanced constraint and is generated with an auxiliary method. The object support contains information about boundaries of the specimen, and thus is a very strong regularizer which significantly reduces missing-cone artifacts and allows for retrieval of full 3D RI distribution. Both algorithms are using first-order Rytov approximation and are designed for the reconstruction of weakly scattering samples. In GPSC, the number of iterations is calculated automatically with a designed stopping criterion, which analyzes the dynamics of the change between 3D reconstructions outputted from consecutive iterations [18], and is usually in the range 10-25 iterations. An example of a GPSC tomographic reconstruction that shows heterogeneous structure of a biological cell is presented in Fig. 1(b).

2.3. Segmentation methods

In order to calculate the average RI value within the whole cell volume and within 2D cross-sections, it is required to apply segmentation techniques. 3D tomographic reconstructions

OPTICS CONTINUUM

were processed using volumetric segmentation based on 3D watershed and rule-based merging algorithm [19,20]. Segmentation was preceded by a preprocessing stage to reduce image artifacts. In the next step, markers for background and biological objects were defined and then superimposed on the original 3D image. Further, the watershed transform was calculated and the results were processed by rule-based merging algorithm, the idea of which was taken from [20]. The goal of the merging technique is to eliminate the over segmentation of cells. Finally, the cell binary mask was created by assigning a value of 1 to all obtained labels. Segmentation was processed on both GPSC and DI reconstruction (see Fig. 2). The binary masks for 2D cross-sections were generated by cross-sectioning the calculated 3D binary mask.

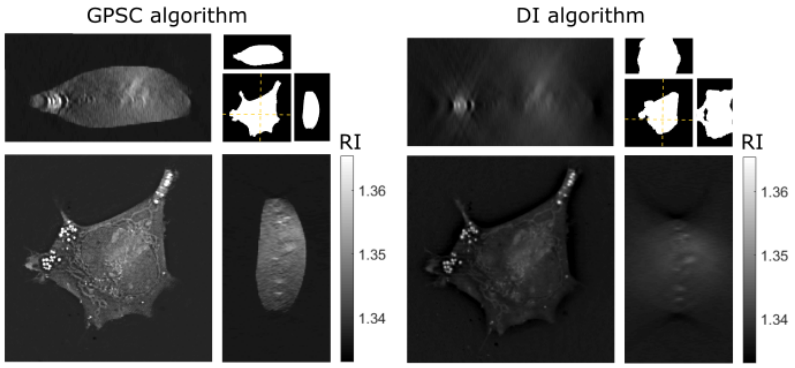

Fig. 2. Tomographic reconstruction of a SH-SY5Y cell calculated with GPSC and DI algorithms shown together with corresponding binary masks generated with 3D watershed and rule-based merging algorithm.

2.4. Cell cultures

In the experiment we measured 3 types of cells: SH-SY5Y neuroblastoma cells, A549 adenocarcinoma lung cells and HL-60 white blood cells. They represent different morphology and properties: SH-SY5Y are aggregating cells, A549 are flat, adherent cells while HL-60 are floating, round cells. All cells were cultured in DMEM/F12 (1:1) medium (PAN Biotech, P04-41450) supplemented with 1% Pen Strep (Gibco, 15140-122), 2 mM L-glutamine (Gibco, 25030-024), 10% heat-inactivated Fetal Bovine Serum (Gibco, 10500-064). Cells were grown under standard conditions (37 °C, 5% CO_2, 90% humidity).

3. Results and discussion

First, in order to show volumetric heterogeneity of biological cells, we calculated high quality 3D tomographic reconstructions of 3 cell lines with the GPSC method. The results are shown in Fig. 3. In the Figure, 2D cross-sections through the reconstructions are presented. We can clearly observe the occurrence of different cell substructures at various heights, e.g. for the A549 cell a cell nucleus is best seen at the cross-section $Z = 68$ ($-1.1\,\mu$m depth with respect to the center of the reconstruction) and lipid droplets at $Z = 12$ and $Z = 55$ ($-8.8\,\mu$m and $-2.9\,\mu$m depth respectively). Similar observations can be made in the case of SH-SY5Y or HL-60 cells.

Next, we compared the average RI calculated from the whole reconstructed volume of cells with the average RI values calculated from 2D lateral cross-sections. The experiment has been conducted for tomographic reconstructions calculated with GPSC and DI methods. The results are aggregated in Fig. 4. Color barplots show the average RI values calculated from each 2D lateral cross-section of a reconstruction generated by the GPSC method, whereas gray barplots represent the same values but calculated with DI algorithm. The horizontal lines represent the

OPTICS CONTINUUM

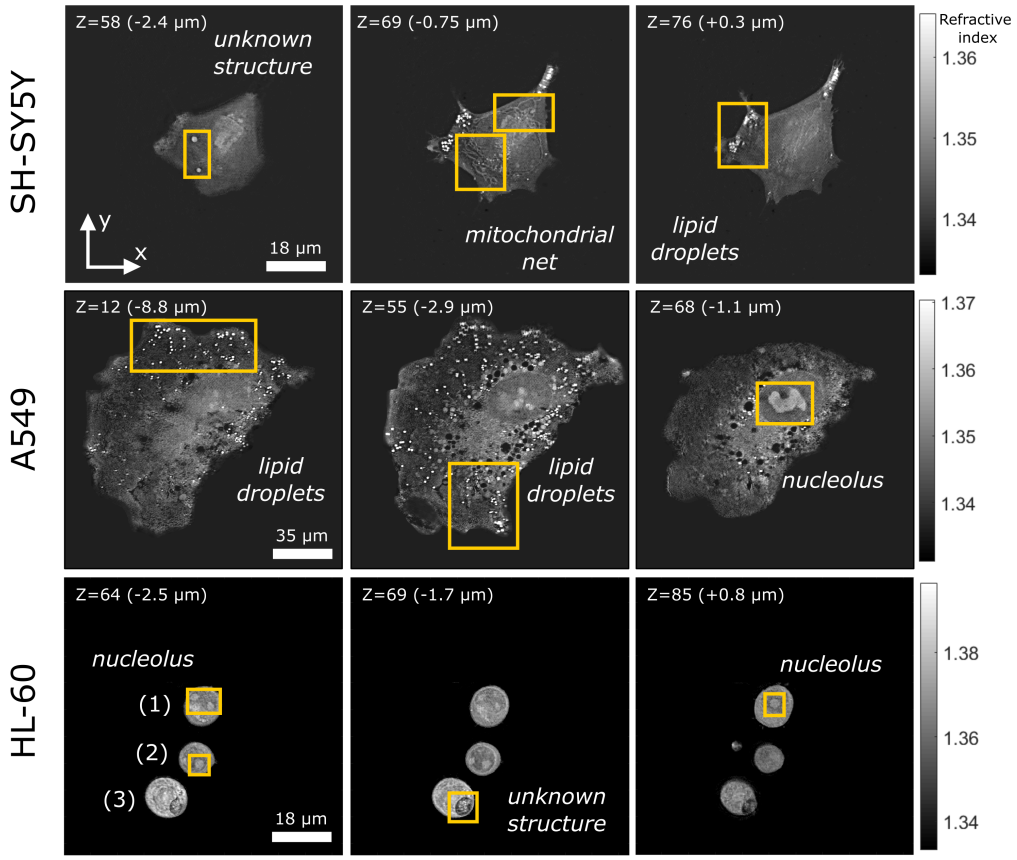

Fig. 3. Cross-sections through GPSC reconstructions of SH-SY5Y, A549 and HL-60 cells. For each cross-section a slice number Z is given together with slice depth given with respect to the center of the reconstruction. Internal organelles visible on different depths were marked with yellow boxes.

average RI value calculated from the whole reconstructed volume. All results are available in Dataset 1 [21].

It can be observed that the 2D cross-section RI values are highly variable depending on the section chosen, which is consistent with the fact that different cell substructures are on different depths (as shown in Fig. 3). Additionally comparing both 2D and 3D RI values calculated from GPSC reconstruction to the values from DI reconstruction it can be easily seen that there is a significant difference in both 2D and 3D RI values - the values calculated with the DI method are underestimated. There are 2 problems with DI reconstructions. Firstly, these reconstructions suffer from severe missing-cone artifacts, one of which is strong elongation of the reconstruction in the z direction. This in turn results in erroneously generated object boundaries with the volumetric segmentation - the calculated volume is much larger (as can be noticed in Fig. 2). Secondly, since the total phase delay encoded in acquired tomographic projections of a biological sample are distributed onto a larger volume, the RI values in each 2D cross-section are lower than true values - even in the central cross-section. This means, that even if one wants to discard the volumetric information obtained with DI method and use only the central cross-section to perform further analysis, the obtained results will not be quantitative and no further analyses based on these values should be performed.

OPTICS CONTINUUM

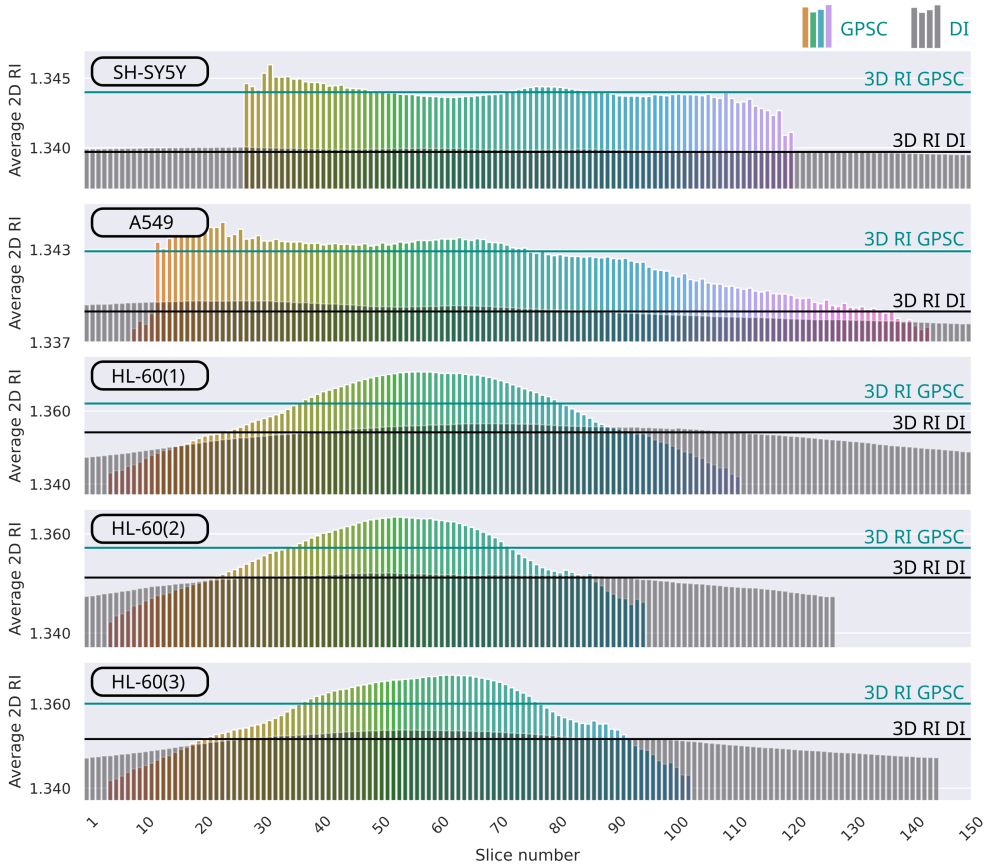

Fig. 4. Comparison of average RI values of 2D slices through tomographic reconstructions (shown with bar plot) of 5 cells with average RI values calculated from the whole 3D reconstruction volume (shown with horizontal line) calculated with GPSC (color barplot) and DI (gray barplot).

These results confirm that when TPM measurements are performed, it is crucial to apply advanced reconstruction procedures that give access to the full volumetric information, like GPSC [11], Learning Tomography [22] or methods that use deep learning [23], even if they are more time- and power-consuming. Otherwise, TPM results cannot be described as quantitative ones.

4. Conclusions

In this paper we show that since biological cells are highly heterogeneous structures, it is crucial to use full volumetric data to calculate the average RI values of biological samples and their organelles. However, in order to obtain high-quality volumetric information it is necessary to employ advanced iterative tomographic reconstruction algorithms, which are addressing the problem of missing cone artifacts. The application of fast reconstruction algorithms, like DI method, or the use of only a single 2D cross-section to calculate RI results in underestimated values that are not acceptable as a quantitative measurement. To prove this claim, we presented results of 5 cells from 3 distinct cell lines. This claim is especially important to communicate in the case of developing quantitative phase imaging techniques, for inter-laboratory studies

OPTICS CONTINUUM

interpretation, building detailed libraries of RI values for biological specimens or developing AI-based diagnostics.

Funding. Narodowe Centrum Badań i Rozwoju (PLTW/V/5/2018); H2020 Industrial Leadership (H2020 Industrial Leadership (101016726)).

Acknowledgments. **MB**: Conceptualization, Data curation, Formal analysis, Investigation, Methodology, Visualization, Writing – original draft. **MM**: Investigation, Writing – original draft. **WK**: Conceptualization, Formal analysis, Funding acquisition, Visualization, Project administration, Supervision, Writing – original draft.

Disclosures. The authors declare that there are no conflicts of interest related to this article.

Data availability. Data underlying the results presented in this paper are available in Dataset 1 [21].

References

1. V. Balasubramani, A. Kuś, H.-Y. Tu, C.-J. Cheng, M. Baczewska, W. Krauze, and M. Kujawińska, "Holographic tomography: techniques and biomedical applications," Appl. Opt. **60**(10), B65–B80 (2021).
2. Y. Sung, W. Choi, C. Fang-Yen, K. Badizadegan, R. R. Dasari, and M. S. Feld, "Optical diffraction tomography for high resolution live cell imaging," Opt. Express **17**(1), 266–277 (2009).
3. S. Lopez-Osorio, Z. D. Velasquez, I. Conejeros, A. Taubert, and C. Hermosilla, "Morphometric analysis of aerobic eimeria bovis sporogony using live cell 3d holotomographic microscopy imaging," Parasitol. Res. **121**(4), 1179–1189 (2022).
4. P. A. Sandoz, C. Tremblay, F. G. van der Goot, and M. Frechin, "Image-based analysis of living mammalian cells using label-free 3d refractive index maps reveals new organelle dynamics and dry mass flux," PLoS Biol. **17**(12), e3000553 (2019).
5. J. Van Rooij and J. Kalkman, "Large-scale high-sensitivity optical diffraction tomography of zebrafish," Biomed. Opt. Express **10**(4), 1782–1793 (2019).
6. M. Baczewska, K. Eder, S. Ketelhut, B. Kemper, and M. Kujawińska, "Refractive index changes of cells and cellular compartments upon paraformaldehyde fixation acquired by tomographic phase microscopy," Cytom. Part A **99**(4), 388–398 (2021).
7. J. Kostencka, T. Kozacki, A. Kuś, B. Kemper, and M. Kujawińska, "Holographic tomography with scanning of illumination: space-domain reconstruction for spatially invariant accuracy," Biomed. Opt. Express **7**(10), 4086–4101 (2016).
8. A. Kuś, W. Krauze, and M. Kujawińska, "Active limited-angle tomographic phase microscope," J. Biomed. Opt. **20**(11), 111216 (2015).
9. W. Krauze, A. Kuś, D. Śladowski, E. Skrzypek, and M. Kujawińska, "Reconstruction method for extended depth-of-field optical diffraction tomography," Methods **136**, 40–49 (2018).
10. J. Lim, K. Lee, K. H. Jin, S. Shin, S. Lee, Y. Park, and J. C. Ye, "Comparative study of iterative reconstruction algorithms for missing cone problems in optical diffraction tomography," Opt. Express **23**(13), 16933–16948 (2015).
11. W. Krauze, "Optical diffraction tomography with finite object support for the minimization of missing cone artifacts," Biomed. Opt. Express **11**(4), 1919–1926 (2020).
12. M. Chen, D. Ren, H.-Y. Liu, S. Chowdhury, and L. Waller, "Multi-layer born multiple-scattering model for 3d phase microscopy," Optica **7**(5), 394–403 (2020).
13. U. S. Kamilov, I. N. Papadopoulos, M. H. Shoreh, A. Goy, C. Vonesch, M. Unser, and D. Psaltis, "Learning approach to optical tomography," Optica **2**(6), 517–522 (2015).
14. A. Géloën, K. Isaieva, M. Isaiev, O. Levinson, E. Berger, and V. Lysenko, "Intracellular detection and localization of nanoparticles by refractive index measurement," Sensors **21**(15), 5001 (2021).
15. Y. Sung and R. R. Dasari, "Deterministic regularization of three-dimensional optical diffraction tomography," J. Opt. Soc. Am. A **28**(8), 1554–1561 (2011).
16. V. Lauer, "New approach to optical diffraction tomography yielding a vector equation of diffraction tomography and a novel tomographic microscope," J. Microsc. **205**(2), 165–176 (2002).
17. A. Kuś, W. Krauze, P. L. Makowski, and M. Kujawińska, "Holographic tomography: hardware and software solutions for 3d quantitative biomedical imaging," ETRI J. **41**(1), 61–72 (2019).
18. W. Krauze, A. Kuś, M. Ziemczonok, M. Haimowitz, S. Chowdhury, and M. Kujawińska, "3d scattering microphantom sample to assess quantitative accuracy in tomographic phase microscopy techniques," Sci. Rep. **12**(1), 19586 (2022).
19. O. Wirjadi, "Survey of 3D image segmentation methods," ITWM Rep. pp. 16–17 (2007).
20. P. S. Umesh Adiga and B. B. Chaudhuri, "An efficient method based on watershed and rule-based merging for segmentation of 3-D histo-pathological images," Pattern Recognit. **34**(7), 1449–1458 (2001).
21. M. Baczewska, W. Krauze, and M. Mazur, "Towards true volumetric refractive index investigation in tomographic phase microscopy at cellular level - dataset," Zenodo, (2022). https://doi.org/10.5281/zenodo.7326417.
22. J. Lim, A. B. Ayoub, E. E. Antoine, and D. Psaltis, "High-fidelity optical diffraction tomography of multiple scattering samples," Light: Sci. Appl. **8**(1), 1–12 (2019).
23. H. Chung, J. Huh, G. Kim, Y. K. Park, and J. C. Ye, "Missing cone artifact removal in odt using unsupervised deep learning in the projection domain," IEEE Trans. Comput. Imaging **7**, 747–758 (2021).